Influence of process parameters on thinning ratio and fittability of bellows hydroforming

Lanfang Jiang[1] · Yi He[2] · Yaochen Lin[3] · Shuyou Zhang[4] · Yixiong Feng[4] · Min Sun[2] · Xunzhong Guo[5]

Abstract

Metal bellows are widely used in piping systems, aerospace, automobile and other industries due to their favourable properties including absorption of expansion, light weight and flexibility. In this paper, the fittability was presented to evaluate the convolution shape precision of the metal bellows. By establishing a finite element model of bellows hydroforming process during the bulging and forming stages, the influence of internal pressure, axial feeding and feeding loading path on the wall thickness variation and fittability of one-convolution bellows was investigated. On that basis, the hydroforming process of multi-convolution bellows was studied, and an experiment was carried out. The results showed that with the increase in internal pressure, the wall thickness of the bellows thinned overall, and the fittability of the root zone of the bellows gradually deteriorated. Some region near the crown zone did not fit the dies well when the internal pressure is small. To improve the fittability of the bellows, the actual axial feeding should be a bit less than the theoretical axial feeding. It is of importance in developing the hydroforming technique and improving the hydroforming quality of bellows.

Keywords Bellows · Hydroforming · Process parameter · Wall thinning ratio · Fittability

1 Introduction

Metal bellows are widely applicable in piping systems, aerospace, automotive and other industries due to their exceedingly anisotropic behaviour, energy absorption of irregular expansion, vibration and mechanical movements, light weight and flexibility [1–4]. The forming methods of such bellows include hydraulic forming, mechanical forming, spinning forming and welding forming [5, 6]. Among them,

hydroforming has become a significant bellows forming process with major advantages including low costs, structural integrity, high precision and efficiency [7–9].

Bellows hydroforming is a complex process with multiple influencing factors, including the tube mechanical properties [10], bellows geometry [9, 11, 12], dies [13–15] and process parameters, and multiple forming defects, such as excessive thinning, cracking, buckling and wrinkling. According to whether the dies can separate or are movable, the bellows

✉ Lanfang Jiang
jlf@zjc.zjut.edu.cn

Yi He
hy960626@163.com

Yaochen Lin
luffy@king-mazon.com

Shuyou Zhang
zsy@zju.edu.cn

Yixiong Feng
fyxtv@zju.edu.cn

Min Sun
sunmincy@163.com

Xunzhong Guo
xunzhong@umich.edu

1 Zhijiang College, Zhejiang University of Technology, Shaoxing 312030, People's Republic of China

2 College of Mechanical Engineering, Zhejiang University of Technology, Hangzhou 310032, People's Republic of China

3 Zhejiang King-Mazon Machinery Co., Ltd., Lishui 321403, People's Republic of China

4 School of Mechanical Engineering, Zhejiang University, Hangzhou 310058, People's Republic of China

5 College of Material Science and Technology, Nanjing University of Aeronautics and Astronautics, Nanjing 211100, People's Republic of China

(a) Initial stage

(b) Bulging stage
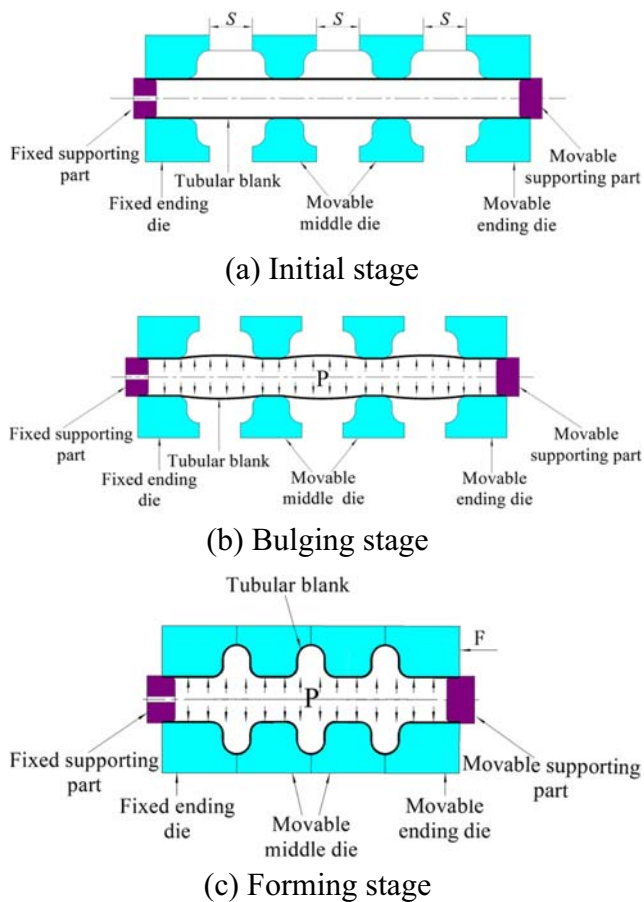
(c) Forming stage

Fig. 1 The principle of the bellows hydroforming process. **a** Initial stage. **b** Bulging stage. **c** Forming stage

hydroforming process was divided into closed-die hydroforming and open-die hydroforming by Elyasi et al. [13], who concluded that closed-die hydroforming is only possible for single-convolution bellows with one end feeding and also possible for a double-convolution bellows with both ends feeding, while there is no limitation on the convolution

number in open-die hydroforming. Therefore, open-die hydroforming is a common forming method for metal bellows.

Some researchers have studied bellows forming in open-die hydroforming. Lee [12] mentioned that the bellows manufacturing process consists of four consecutive processes: deep drawing, ironing, tube bulging and folding. The two stages of tube bulging and folding are critically important. The effects of wall thickness, internal pressure and die stroke on the displacement of the crown point and inner point were examined. Faraji et al. [10, 16] studied the effect of die stroke, internal pressure, mechanical behaviour of tube material and axial displacement on thickness variation, crown diameter and length of the bellows after spring back. The results pointed out that the internal pressure is one of the most important parameters in forming metal bellows. Bakhshi-Jooybari et al. [3] studied the effect of internal pressure path on forming bellows and obtained a comprehensive forming window and the safe zone without wrinkling or bursting in the bulging and closing stages. Yuan et al. [11] investigated the influence of hydraulic pressure, waveform parameters, initial wall thickness and number of layers on the residual plastic strain and wall thickness thinning of reinforced S-shaped bellows. The research showed that the control of hydraulic pressure is a key factor in hydroforming. Zhu et al. [17] proposed hydroforming with axial feeding by using movable dies for complicated thin-walled circular superalloy parts, and the effect of forming area height for the cylinder blank and loading paths of the cavity pressure on the excessive wall thinning, accumulation folding and configurational asymmetry were discussed. Liu et al. [18] studied the influence of internal pressure, die stroke, loading path and axial feeding rate on the deformation behaviours of bi-layered 304 stainless steel bellows. The results showed that the internal pressure and die stroke are the main parameters that affects the wall thinning and convolution height. Zheng et al. [15] analysed the influence of internal pressure, die fillet
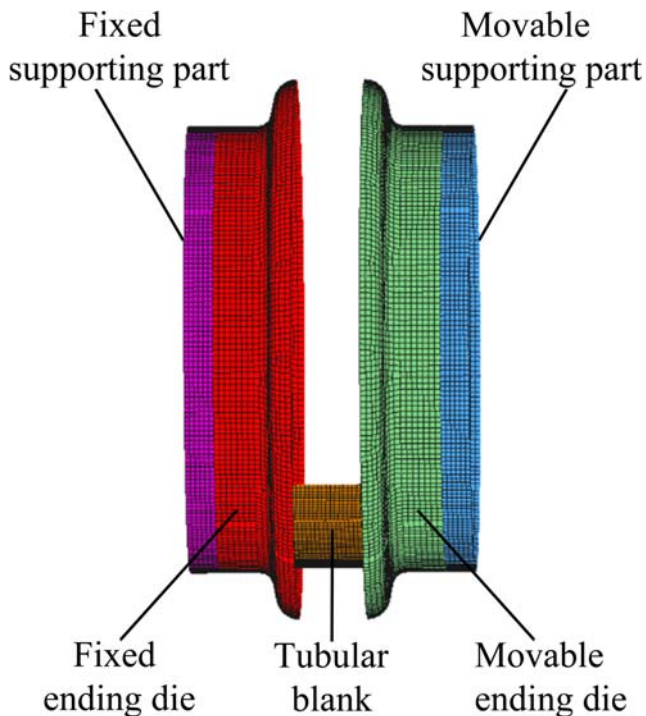
Fig. 2 Geometry of bellows
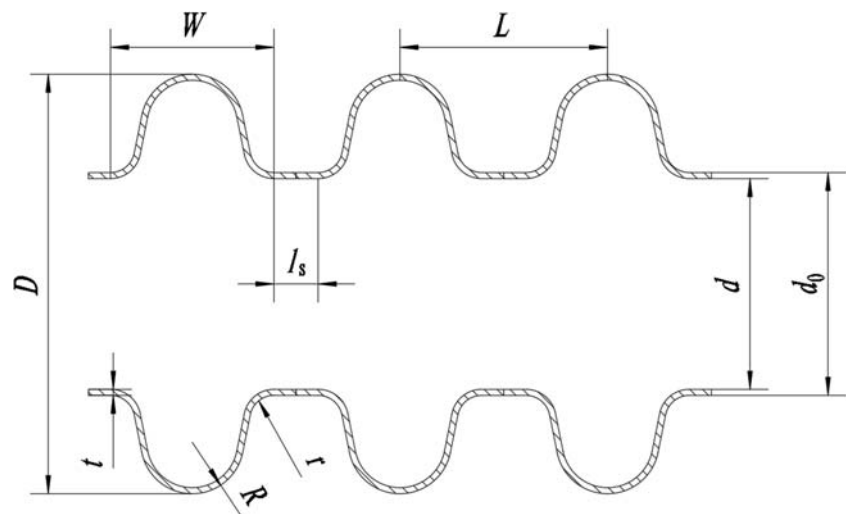
Table 1 Geometric parameters of bellows

Parameter	Value
Tube outer diameter, d_0 (mm)	31
Tube inner diameter, d (mm)	29.7
Wall thickness, t (mm)	0.65
Convolution outer diameter, D (mm)	37.5
Root radius, r (mm)	1
Crown radius, R (mm)	1.5
Convolution width, W (mm)	5.4
Pitch of convolution, L (mm)	8
Straight edge length, l_s (mm)	2.6

Table 2 Mechanical properties of 304 stainless steel tubular blank

Parameter name	Value
Density, ρ (g/cm3)	7.85
Young's modulus, E (Gpa)	195.3
Poisson's ratio, υ	0.285
Yield stress, σ_s (Mpa)	256
Tensile strength, σ_b (Mpa)	520
Pre-strain, ε_0	0.0662
Strain hardening exponent, n	0.72
Strength factor, K (Mpa)	1667.7

size and die spacing on maximum reduction rate and spring back of bellow hydroforming.

In recent years, some researchers proposed new forming methods for bellows [4, 5, 19–22]. Hao et al. [19] proposed an improved hydraulic bulging process with axial feeding in bulging procedure. The process contains three procedures: (a) positioning, (b) bulging and (c) folding. The results showed that the wall thickness distribution of the bellows was more uniform. However, the process should repeat the procedure from (a) to (c) to achieve single waveform continuous forming. Zhang et al. [5, 20] developed a new superplastic forming method of utilizing high-temperature gas instead of oil to create internal pressure for U-type two-convolution titanium alloy bellows. The influence of loading path and length of the tubular blank on the thickness distribution was
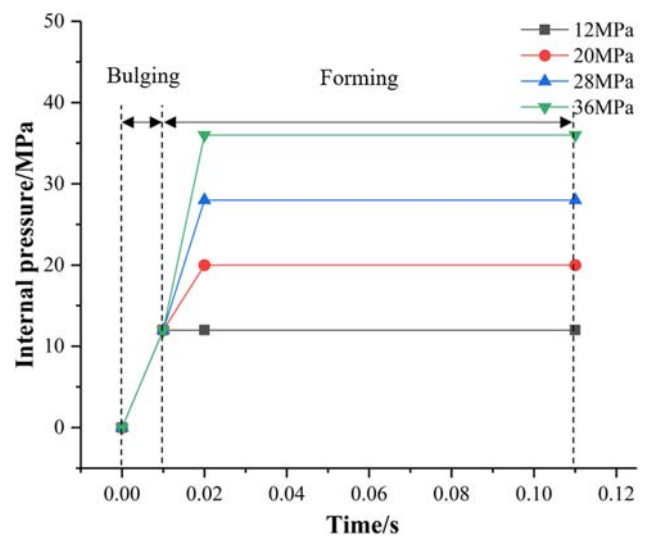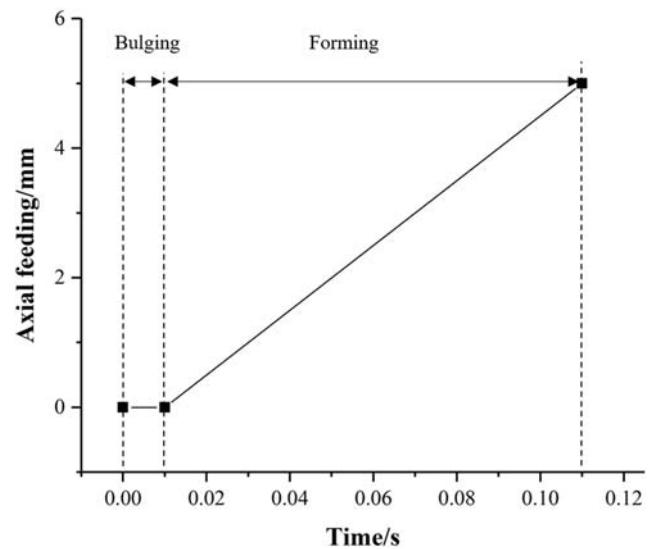
performed. They also pointed out that the key points of the new superplastic forming process are the matching between

(a) The loading path of the internal pressure

(b) The loading path of the axial feeding

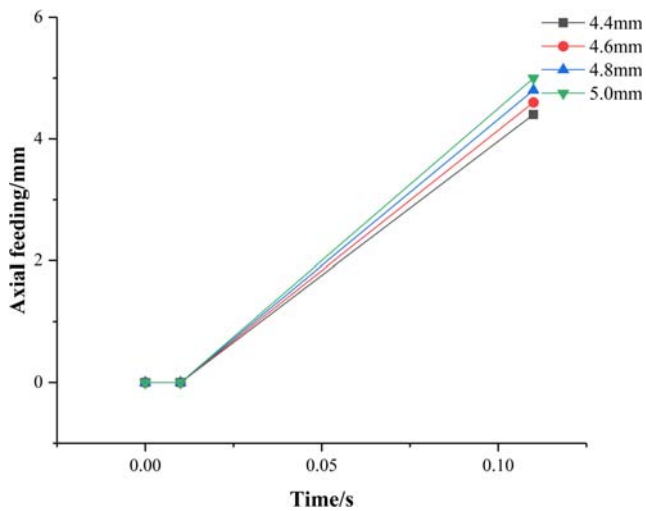**Fig. 4** Loading path of the FE analysis. **a** Internal pressure. **b** Axial feeding

Fig. 3 Finite element meshed model

Fig. 5 Loading path of the axial feeding

Fig. 6 Combined axial feeding loading path in hydroforming

the inner forming pressure and time during the bulging stage, and the gas pressure during the shape forming stage. Wei et al. [4] presented a new water jet incremental forming technology, with where bellows were formed with a nozzle and no die is needed. With the nozzle rotating in circle, the outline of bellows can be manufactured. Zhang et al. [21] proposed a dieless metal bellows forming process using a local heating technique and axial compression. They found that the convolution height can be controlled by the compression ratio. Sedighi et al. [22] introduced a new local heating method in dieless metal bellows forming using simultaneous local electric arc heating on the rotating tube and axial compression.

From the above studies, it can be concluded that many researchers have focused their attention on the effect of forming parameters of internal pressure, axial feeding and die stroke on bellows quality, as evaluated by wall thickness, convolution height and length of the bellows after spring back. The wall thickness variation has a significant effect on the quality and performance of bellows, while the convolution shape precision also influences the forming quality and practical performance of bellows. However, little research has been performed on this topic. Some researchers have studied the convolution height, and the displacements of the crown
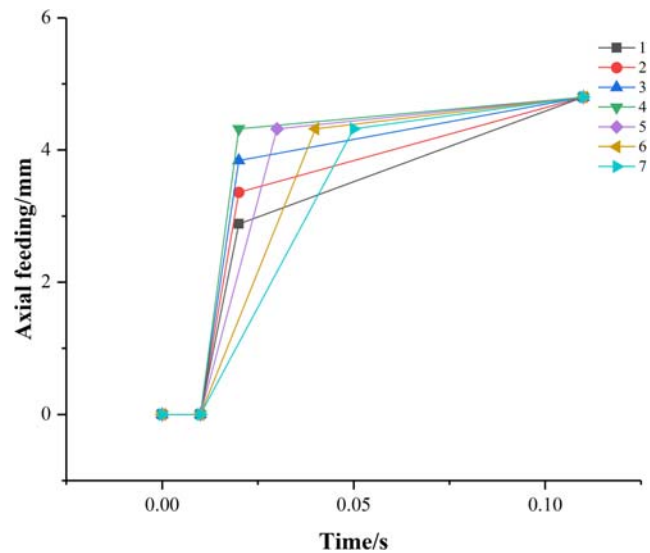
and inner points, but this cannot fully reflect the convolution shape precision of the bellows. Therefore, it is important to investigate the convolution shape precision of the bellows in the hydroforming process.

The above recently proposed new forming methods for bellows do not easily ensure the convolution shape precision of the bellows, because there is no die cavity with a corresponding shape [4, 21, 22], although the convolution height can be controlled. In addition, some new methods can manufacture convolution only one by one, with low efficiency [4, 19, 21, 22]. Some new methods that use heating techniques require complex process and high costs [6, 20–22].

In this paper, the fittability is presented to evaluate the convolution shape precision of the metal bellows. A finite element (FE) model of the bellows hydroforming process during the bulging and forming stages is established. The influence of important process parameters, including internal pressure, axial feeding and feeding loading path, on wall thickness variation and fittability of the metal bellows is investigated. An experiment is carried out to verify the numerical analysis.

2 Principle of metal bellows hydroforming process

The principle of the bellows hydroforming process is shown in Fig. 1. It is performed with fixed supporting part, fixed ending dies, movable middle dies, movable ending dies and movable supporting part. The process includes three stages:

(1) Initial stage: the forming dies are placed outside of the tube at an equal distance. The tube is sealed at the two ends by the supporting parts. The initial distance between

Table 3 Combined feeding loading path in the early period

Path no.	Axial feeding time T_{f1}	Axial feeding S_1
1	$0.1T_f$	$0.6S$
2	$0.2T_f$	$0.7S$
3	$0.3T_f$	$0.8S$
4	$0.4T_f$	$0.9S$
5	$0.2T_f$	$0.9S$
6	$0.3T_f$	$0.9S$
7	$0.4T_f$	$0.9S$

Fig. 7 Wall thickness distributions of the bellows
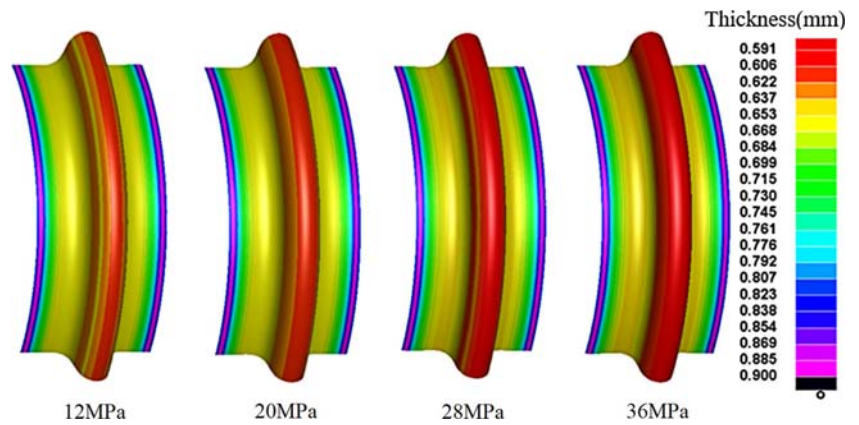
dies (also called the die stroke) is determined according to the convolution structure.

(2) Bulging stage: the internal pressure is applied, and the value increases until the tube is slightly bulged. No axial feeding is applied to the dies in this stage.

(3) Forming stage: axial displacement feeding is applied to the movable ending dies while the internal pressure is maintained. Under the action of internal pressure and axial feeding, the dies close together and form the final shape of the bellows. In addition, the movable supporting part moves with the end of the tube.

3 FE model

3.1 Geometric modelling

The geometry of bellows is shown in Fig. 2. The geometric parameters are listed in Table 1. To improve the computational efficiency, a 1/4 model is chosen considering the symmetry of the bellows and dies.

The 304 stainless steel tube with outer diameter of $d_0 = 31$ mm and wall thickness of $t = 0.65$ mm will be bulged, forming the bellows with a convolution outer diameter $D = 37.5$ mm. According to the principle of constant volume before and after bulging, the initial deformation zone length of tubular blank for one convolution is determined to be 10.38 mm. Adding the length of the straight edge l_s and considering the trimming margin, the initial length of the tubular blank is finally determined to be 15.8 mm.

3.2 Element and mesh

The FE model is conducted with DYNAFORM software. The dies and supporting parts are modelled using the actual dimensions of the working surface. The tube is modelled using a neutral layer size. The thin shell Belytschko-Tsay (BT) is used to mesh the tube and dies. The mesh properties have an important influence on the accuracy of numerical simulations. The better the mesh quality, the higher the accuracy of the
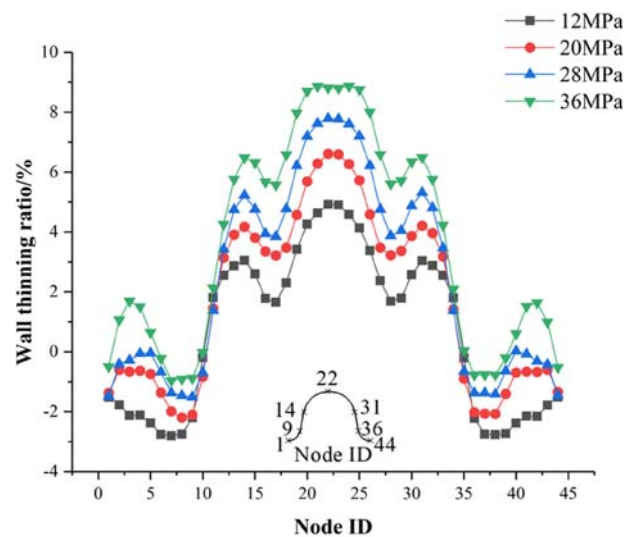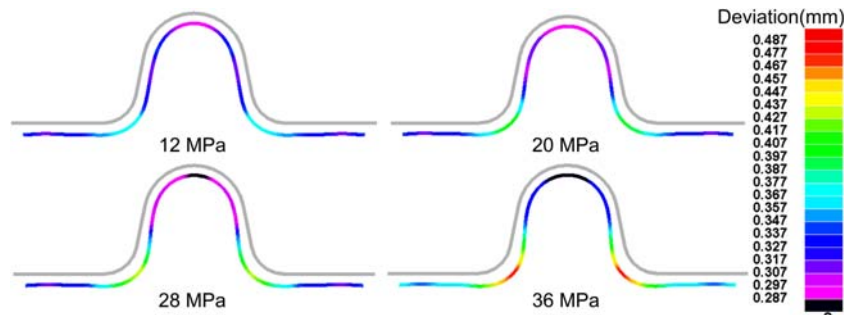

(a) Wall thinning ratio at nodes
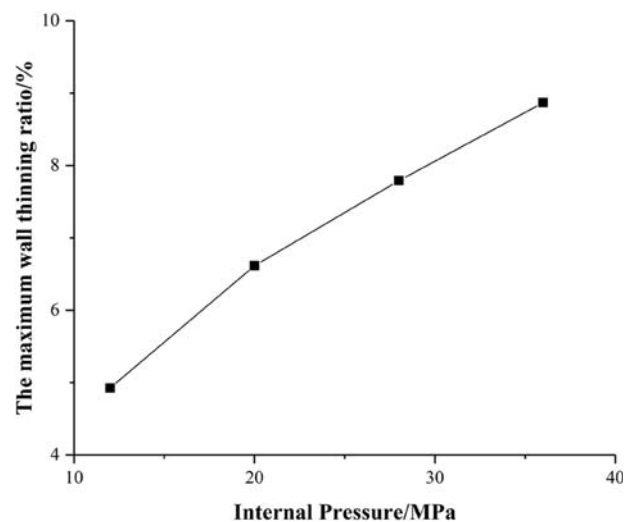
(b) The maximum wall thinning ratio of the bellows

Fig. 8 Variation curves of the wall thinning ratio under different internal pressures. **a** Wall thinning ratio at nodes. **b** The maximum wall thinning ratio of the bellows

Fig. 9 Deviation under the four different internal pressures

simulation result. However, the number of mesh should be controlled within a certain range to improve the calculation efficiency. The meshed model with a total of 33,960 elements is shown in Fig. 3.

3.3 Material

The transversely anisotropic elastic-plastic material model is selected to describe the constitutive relation for the tube material. The HW Swift enhancement equation for the material model is as follows:

$$\sigma = K(\varepsilon + \varepsilon_0)^n \tag{1}$$

where σ is the equivalent stress, ε is the equivalent plastic strain, ε_0 is the pre-strain, K is the strength factor, and n is the strain hardening exponent.

The mechanical properties of 304 stainless steel materials are listed in Table 2.

3.4 Boundary conditions

In the numerical simulation, the deformation of the forming dies is neglected. Therefore, the dies and supporting parts are set as rigid bodies. All the DOFs of the fixed supporting part and fixed ending dies are constrained. Only the DOF of the movable dies and supporting part in the axial direction of the tube is retained. The axial displacement feeding is defined at the end of the movable ending dies. The internal pressure is applied on the internal surface of the tube. For the 1/4 model, it is necessary to apply the symmetrical constraints on the tubular blank.

The numerical simulation of the bellows hydroforming process is mainly the contact between the dies and tubular blank, and whether there is penetration between them is not considered. The contact between the dies and tubular blank is single-sided, and the contact method is one way surface-to-surface. Here, the penetration of the tubular blank node into a die mesh surface is considered. That is, the tube is the slave

surface, and the concave die is the main surface. The single-sided contact is set as the non-automatic single-sided contact. The Coulomb friction model is used to describe the friction and the friction coefficient between the dies and tube is 0.125. For bellows hydroforming involving large deformation and dynamic contact problems, the dynamic explicit algorithm is adopted for the bulging and forming stages. Using the FE software DYNAFORM, an FE model of bellows hydroforming during the bulging and forming stages is established. Based on this model, the hydroforming process is simulated, and the results are analysed.
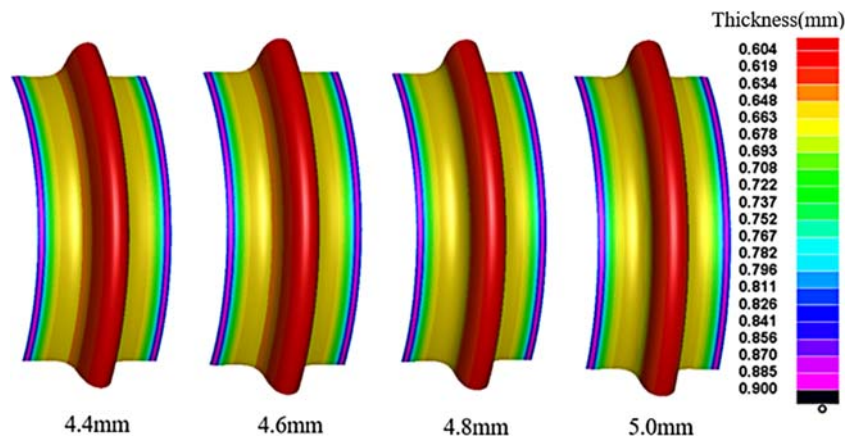
4 Numerical calculation and result analysis

4.1 Research scheme

This section mainly investigates the influence of the internal pressure, axial displacement feeding and feeding loading path
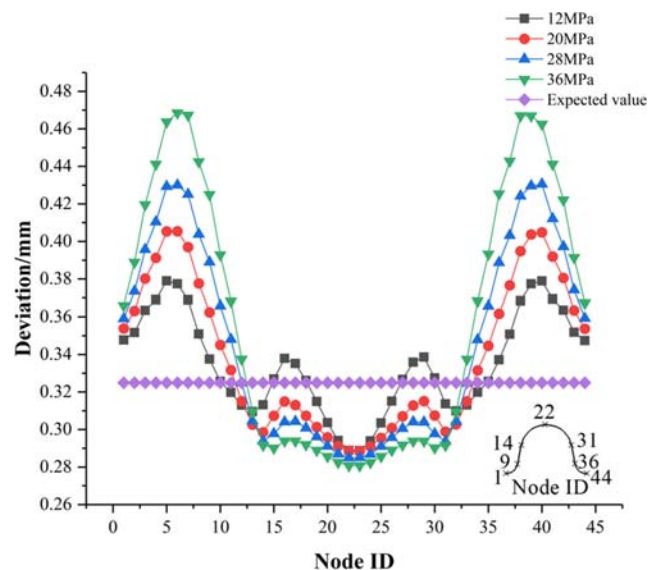
Fig. 10 Variation curves of the deviations at the nodes

Fig. 11 Wall thickness distributions of the bellows under the different axial feedings

on the wall thickness variation and fittability of one-convolution bellows in the hydroforming process. The specific scheme used in this research is as follows.

4.1.1 Internal pressure for hydroforming

The yield internal pressure and ultimate internal pressure of the tube should be determined first. By using the thin-wall pressure vessel theory, the theoretical internal pressure necessary to start the bulging process can be determined by Eq. (2) [8], and the ultimate internal pressure can be determined by Eq. (3) [23]:

$$P_s = \frac{2\sigma_s t}{d} \tag{2}$$

$$P_b = \frac{4\sigma_b t}{d} \tag{3}$$

where P_s is the yield internal pressure, P_b is the ultimate internal pressure, σ_s is the yield stress of the tubular blank, σ_b is the tensile strength of the tube, t is the initial wall thickness of the tube and d is the inner diameter of the tube. From the formulas, the theoretical yield internal pressure and ultimate internal pressure can be calculated, which are 11.2 MPa and 45.52 MPa, respectively.

The actual yield internal pressure should be greater than the theoretical yield internal pressure. After many previous simulation studies, the actual yield internal pressure P_s in the bulging stage is determined to be 12 MPa. That is, the internal pressure increases linearly from 0 to 12 MPa in a short time in the bulging stage.

In the forming stage, the internal pressure is maintained while the axial feeding is applied to the movable ending dies. To study the influence of the internal pressure on the forming quality of bellows, four values are chosen for the forming internal pressure P_f, 12 MPa, 20 MPa, 28 MPa and 36 MPa. The loading path of the internal pressure adopts a gradient loading path with the proportion of increasing time to holding time of 1:9.
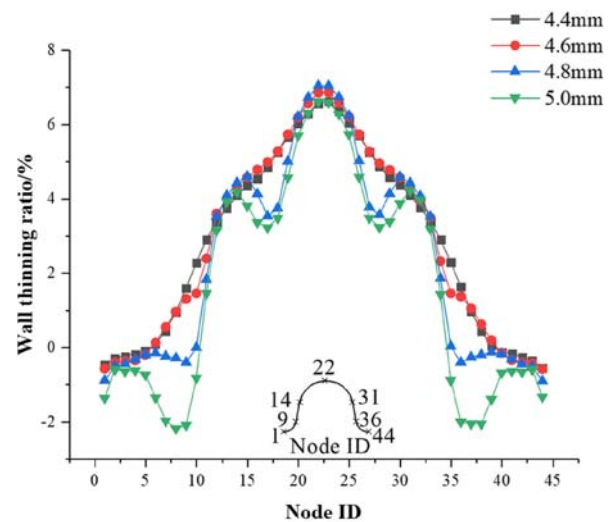

(a) Variation curves of the wall thickness thinning ratio at nodes
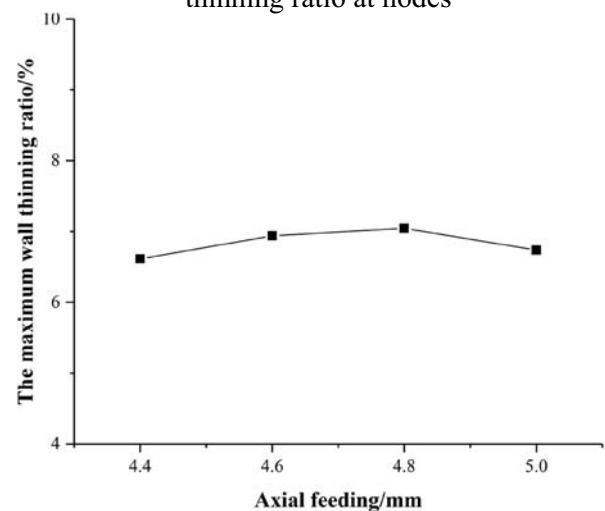
(b) The maximum wall thinning ratio of the bellows

Fig. 12 The wall thinning ratios of the bellows under different axial feedings. **a** Variation curves of the wall thickness thinning ratio at nodes. **b** The maximum wall thinning ratio of the bellows

Fig. 13 Deviation from the bellows to dies under the four different axial feedings
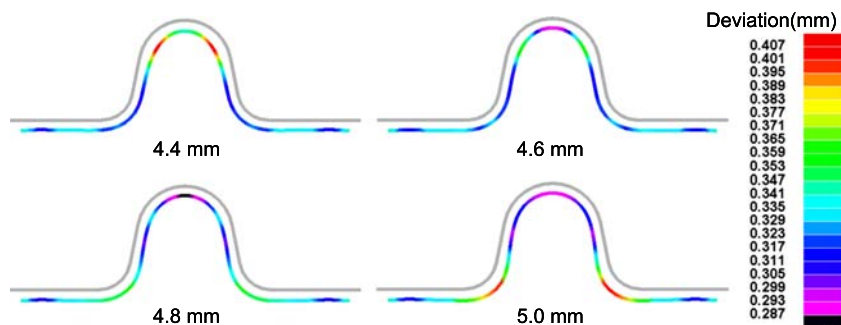
Meanwhile, the axial feeding adopts a linear loading path. The axial feeding is equal to the initial distance between dies for one-convolution bellows. The theoretical value equals the length of one-convolution expansion minus the convolution width, expressed as follows:

$$S = L_0 - W \tag{4}$$

where S is the axial feeding, which equals the distance between dies (also called die stroke); L_0 is the length of one convolution expansion, which equals the initial deformation zone length of tubular blank for one convolution; and W is the convolution width. Then, the axial feeding of displacement is calculated as 4.98 mm.

Considering that simulating the actual time loading will make the calculation take too long and produce a low efficiency, the virtual time loading is $T = 0.11$ s, where the time for the bulging stage $T_b = 0.01$ s and the time for the forming stage $T_f = 0.1$ s. The virtual loading time and proportion of the bulging and forming stage lengths are all the same in the following studies. The loading path of the internal pressure is shown in Fig. 4a, and the loading path of the axial feeding is shown in Fig. 4b.

4.1.2 Axial feeding

For a given tubular blank and designed die shape, excessive axial feeding may cause wrinkling in the deformation zone and insufficient axial feeding may lead to excessive thinning and even bursting in the large expansion zone. Based on the theoretical value of axial feeding, four values are chosen for the axial feeding S, including 5 mm, 4.8 mm, 4.6 mm and 4.4 mm, to investigate the influence of axial feeding on the forming quality of bellows. The axial feeding still adopts a linear loading path, as shown in Fig. 5.
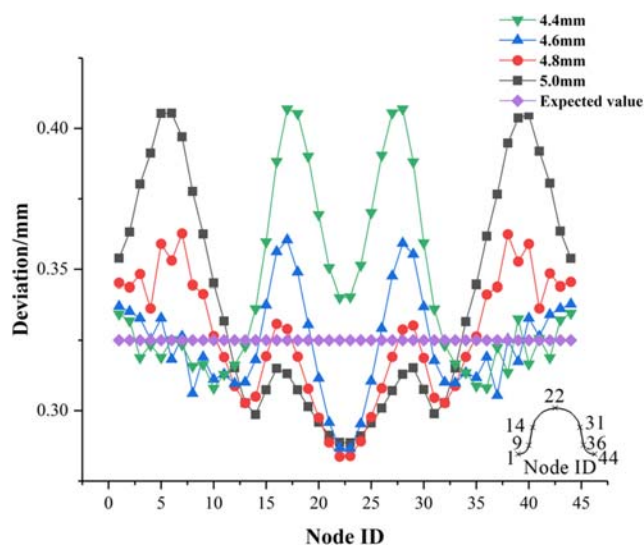
4.1.3 Feeding loading path

Studies have shown that under the same axial displacement feeding condition, rapid feeding at the beginning of the

forming stage is beneficial to reduce the wall thinning ratio of bellows [24]. Therefore, bilinear loading paths are designed with different rapid feeding in the early period to study the influence of the feeding loading path on the forming quality of the bellows. Four values are designed for the axial feeding time in the early period T_{f1}, including $0.1T_f$, $0.2T_f$, $0.3T_f$ and $0.4T_f$, and four values are designed for axial feeding of displacement in the early period S_1, including $0.6S$, $0.7S$, $0.8S$ and $0.9S$. To generate a large difference in the feeding between early period and later period, seven combined schemes of axial feeding time and axial feeding are designed, as listed in Table 3, and the combined axial feeding loading is shown in Fig. 6.
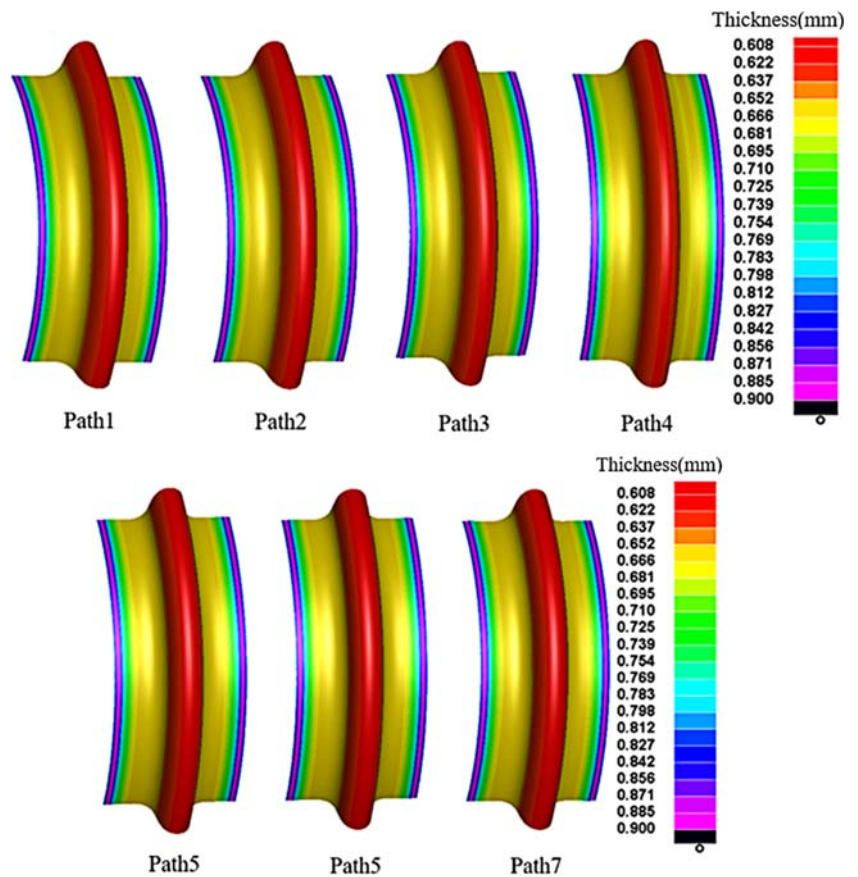
4.2 Evaluation indicators

In this study, the wall thinning ratio and fittability of the metal bellows are used as important indicators to evaluate the forming quality of the bellows.

Fig. 14 Variation curve of the deviation at the nodes under the four different axial feedings

Fig. 15 Wall thickness distributions of the bellows under different feeding loading paths

4.2.1 Wall thinning ratio

The wall thinning ratio is an important evaluation indicator influencing the hydroforming quality of the bellows. An excessive wall thinning ratio will seriously affect the performance and useful life of the bellows. The wall thinning ratio is expressed as follows:

$$\delta = \left| \frac{t - t_h}{t} \right| \times 100\% \tag{5}$$

The maximum wall thinning ratio is as follows:

$$\delta_{max} = \left| \frac{t - t_{min}}{t} \right| \times 100\% \tag{6}$$

Table 4 The maximum wall thinning ratio of the bellows under different axial feed paths

| Path no.	Maximum wall thinning ratio
1	5.63%
2	5.32%
3	5.03%
4	4.65%
5	5.8%
6	6.17%
7	6.49%

where δ is the wall thinning ratio, δ_{max} is the maximum wall thinning ratio, t_h is the wall thickness of the bellows and t_{min} is the minimum wall thickness of the bellows.

4.2.2 Fittability

Fittability is another important indicator used to evaluate the forming quality of metal bellows after hydroforming. Before the hydroforming process, the die cavity is designed into a shape corresponding to the convolution to ensure convolution shape precision. Fittability is the ability of tubular blank to fit the die cavity and obtain the die shape during the hydroforming process. Thus, fittability evaluates the forming quality of the bellows from the perspective of the convolution shape precision of the bellows.

In operations, the ideal deviation from the neutral layer of bellows to the dies under the ideal state in which the bellows completely fit the die cavity and obtain the die shape is set as the expected value; the actual deviation from the neutral layer to the dies after hydroforming is set as the actual value. The closer the actual value is to the expected value, the higher the convolution shape precision, and the better the forming quality of the bellows.

Fig. 16 Deviation from the bellows to dies under the seven different feeding loading paths
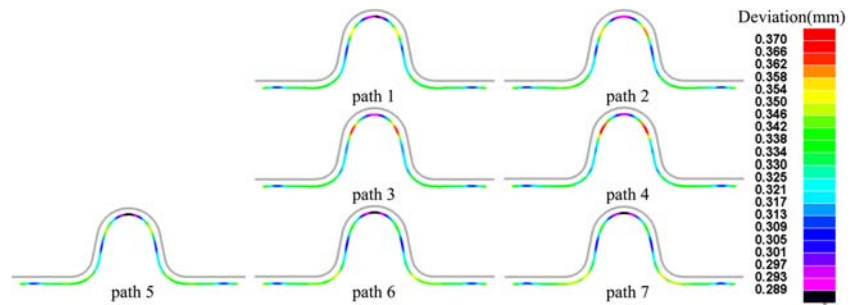

4.3 Results and analysis

4.3.1 Influence of internal pressure

Figure 7 shows the wall thickness distributions of the bellows under different internal pressures. Figure 8a shows the variation curves of the wall thinning ratio at nodes, and Fig. 8b shows the maximum wall thinning ratios of the bellows.

It can be observed from Fig. 7 that wall thinning mainly occurs in the crown zone and the straight wall zone between the crown and root. It can be seen from Fig. 8a that the wall thinning ratios show an overall increasing trend from the root to the crown. The maximum thinning ratio occurs at the crown position. Comparing the wall thinning ratio under the different internal pressure, it can be concluded that with the increase in internal pressure, the overall wall thinning ratio increases as well. When the internal pressure is 12 MPa, the wall thickens obviously in the root zone, which may cause wrinkling. The maximum wall thinning ratio of the bellows increases linearly with increasing internal pressure, as shown in Fig. 8b. This result arises because the increase in internal pressure increases the circumferential and axial stress on the tube material.

The tubular blank is modelled using the neutral layer, so the expected value between the neutral layer of the bellows and the dies is 0.325 mm. Figure 9 shows the deviations under the four different internal pressures, and Fig. 10 shows the variation curves of the deviations at the nodes. In Fig. 9, the actual values between the sections of bellows and the dies are smaller than the expected value near the crown zone. This is because the initially neutral layer and the intermediate layer of the tubular blank are coincident before hydroforming. As the tubular blank gradually bulges to form the bellows, the wall thickness thins, and the neutral layer deviates. Figure 9 shows that the crown zone and the straight wall zone have good fittability, while the root zone has poor fittability under different internal pressures. It can be observed from Fig. 10 that with the increase in internal pressure, the fittability of the root zone of the bellows gradually deteriorates. Some region near the crown zone did not fit the dies well when the internal pressure is small (12 Mpa). When the internal pressure increases, the crown zone could completely fit the dies. This is because the larger internal pressure results in more serious

bellows wall thinning. The theoretical value of axial feeding is adopted in this section, which is greater than actually needed. After fitting the die cavity, the excess material will be squeezed into the root zone due to the restriction of the dies and supports, which causes the root zone to sag with poor fittability.
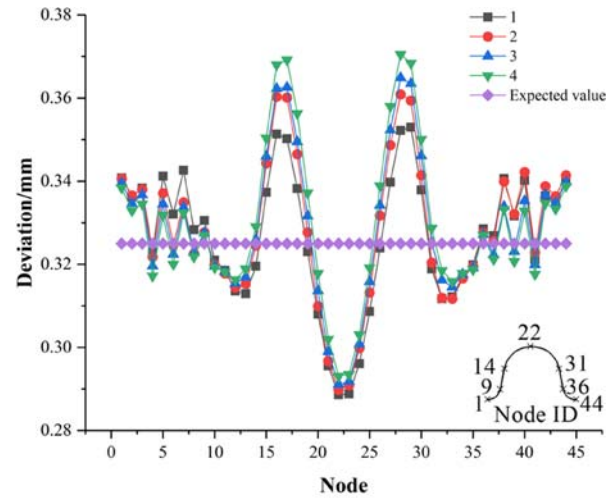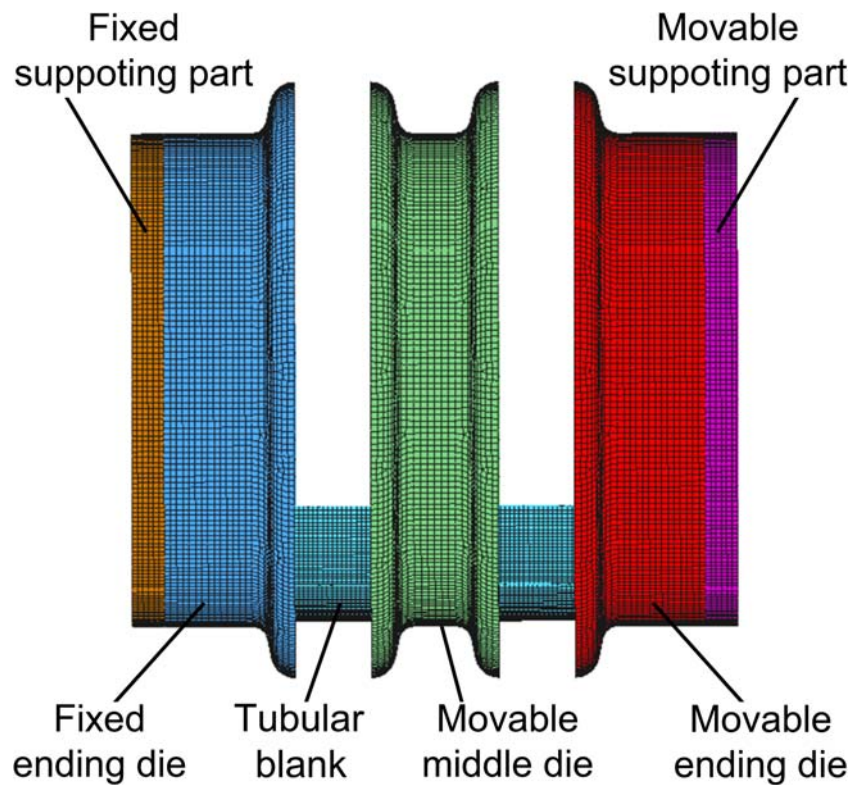

(a) Path 1-4
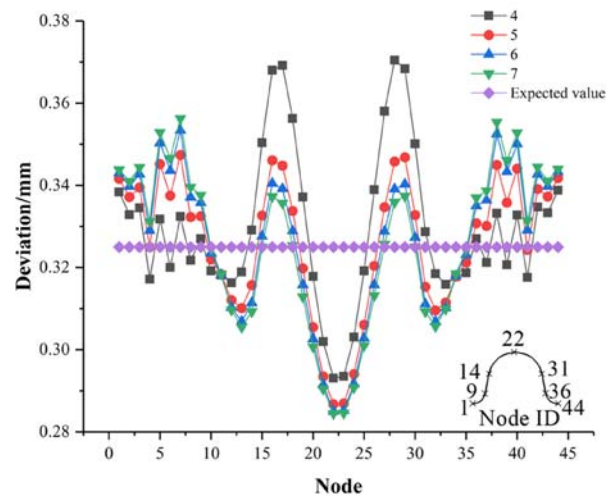
(b) Path 4-7

Fig. 17 Variation curve of the deviations at the node. **a** Paths 1–4. **b** Paths 4–7

Fig. 18 FE model of two-convolution bellows

In addition, when the internal pressure is 12 MPa, the fittability of the crown zone is unstable at nodes due to the deviations from the expected value, which is considered to represent a poor fittability. Combining the influences on wall thickness variation and fittability, the value of 20 MPa for internal pressure is the best among the four different values considered.

4.3.2 Influence of axial feeding

The loading path of internal pressure adopts the gradient loading path with a yield internal pressure P_b value of 12 MPa in the bulging stage and a forming internal pressure P_f value of 20 MPa to study the influence of axial feeding in this section. Figure 11 shows the wall thickness distributions of the bellows under the different axial feedings. Figure 12a shows the variation curves of the wall thinning ratio at nodes, and Fig. 12b shows the maximum wall thinning ratio of the bellows. It can be observed from Fig. 11 that when the axial feeding is smaller (less than 4.6 mm), the wall thinning in the root zone becomes slightly worse, and the thinned area becomes larger.

In Fig. 12a, with the increase in the axial feeding, the wall thinning ratio in some zones decreases, but has little effect on the maximum wall thinning ratio of the bellows in Fig. 12b. This is because as the axial feeding increases, the material in the bellows deformation region increases as well, so the wall thinning ratio can decrease. It can also be observed from

Fig. 12a that when the axial feeding is 5 mm, the wall thickens near the root zone and has a tendency of wrinkling. Therefore, it can be concluded that with the increase in the axial feeding, the wall thinning ratio in some zones decreases, but the wall thickens near the root zone with a tendency of wrinkling.

Figure 13 shows the deviations from the bellows to dies under the four different axial feedings, and Fig. 14 shows the variation curves of deviations at the nodes. It can be seen from Figs. 13 and 14 that when the axial feeding is smaller (less
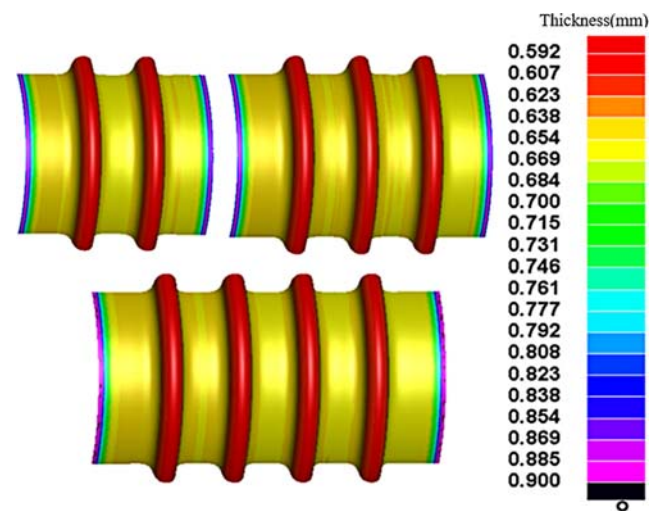

Fig. 19 Wall thickness distributions of the bellows with different convolution number
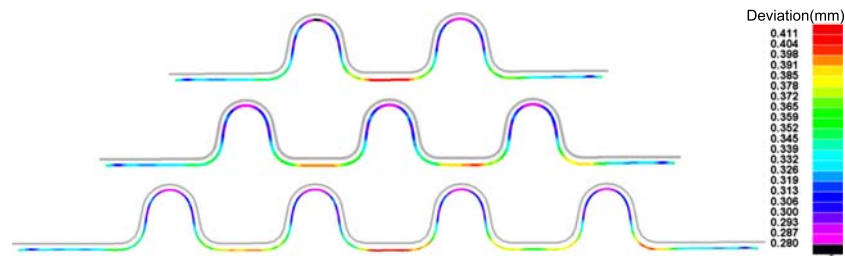
Fig. 20 Deviation from the bellows to dies with different convolution number

than 4.6 mm), the fittability of the two sides of the crown is poor. With the increase in axial feeding, the fittability of the crown zone gradually improves; however, the fittability of the root zone gradually worsens, especially when the axial feeding is greater than 4.8 mm. This is because increasing the axial feeding will increase the material in the deformation zone, and the fittability at the crown zone improves. After fitting the dies in the crown zone, excessive material is transferred to the root zone, causing material accumulation and depression, and the fittability worsens. Combining the influences of axial feeding on wall thickness variation and fittability, it can be concluded that by reducing the axial feeding, the maximum wall thinning ratio of the bellows does not change much, but the foldability changes greatly. Therefore, to improve the fittability of the bellows, the actual axial feeding should be a bit less than the theoretical axial feeding. The value of 4.8 mm for axial feeding is the best among the four different values considered.

4.3.3 Influence of feeding loading path

In this section, the loading path of internal pressure adopts a gradient loading path with a forming internal pressure P_f value of 20 MPa, and the axial feeding adopts a linear loading path with a value 4.8 mm to investigate the influence of axial feeding loading path. Figure 15 shows the wall thickness distributions of the bellows under different feeding loading paths. The maximum wall thinning ratio of the bellows is listed in Table 4. It can be seen from Fig. 15 that under different feeding loading paths, the wall thinning ratio of the

bellows rarely changes. It can be seen from Table 4 that when the axial feeding in the early period is constant, the larger the axial feeding is, the smaller the maximum wall thinning ratio. When the axial feeding is constant, the shorter the feeding time is, the smaller the maximum wall thinning ratio. Therefore, it can be concluded that when the axial feeding adopts a bilinear loading path in the bellows hydroforming process, the larger the axial feeding rate in the early period, the smaller the maximum wall thinning ratio.

Figure 16 shows the deviations from the bellows to dies under the four different feeding loading paths, and Fig. 17 shows the variation curves of the deviations at the nodes. It can be seen from Fig. 16 that the trends of the fittability of the bellows under different feeding loading paths are basically the same. That is, the fittability gradually improves from the root

Fig. 21 Hydroforming bellows and two halves
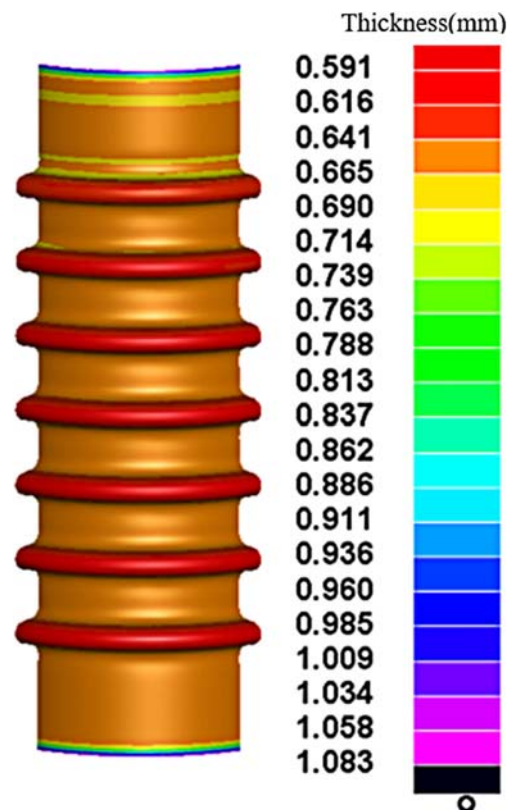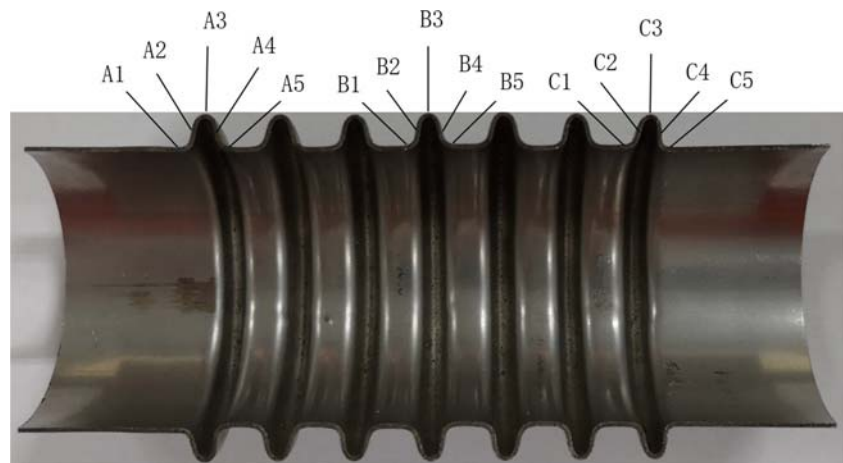

Fig. 22 Wall thickness distributions of the seven-convolution bellows

Fig. 23 Wall thickness of five key points

to the straight wall between the root and crown, gradually worsens from the straight wall to the crown and then gradually improves as it approaches the crown. As seen from Fig. 17, comparing paths 1, 2, 3 and 4, the fittability of the root zone gradually improves slightly, and the fittability close to the crown zone gradually worsens considerably. Comparing paths 4, 5, 6 and 7, the fittability of the root zone gradually worsens slightly, and the fittability close to the crown zone gradually improves more considerably. The variation tendencies of paths 5, 6 and 7 are larger compared with those of paths 1, 2, 3 and 4. This finding illustrates that when the internal pressure and axial feeding are constant, with the increase in axial feeding rate in the early period, the fittability of the bellows roots gradually improves slightly, while the fittability close to the crown zone gradually worsens considerably. The greater the differences in axial feeding rate in the early period, the more obvious the trend.

## 5 Application to multi-convolution bellows

5.1 Multi-convolution single-step hydroforming

To study the multi-convolution single-step hydroforming method, the metal bellows hydroforming process with convolution numbers 2 to 4 is simulated and analysed. The axial feeding of the movable ending dies equals $4.8 * n_c$ mm, where n_c is the number of the convolution. Path 5 is selected for the feeding loading path. The loading path of internal pressure adopts a gradient loading path. To ensure the bellows quality with multi-convolution, the forming internal pressure is determined to be 36 MPa after many preliminary simulations. Figure 18 is the FE model of two-convolution bellows hydroforming. The FE models of three-convolution bellows and four-convolution bellows also can be obtained by adding movable middle dies.

Figure 19 shows the wall thickness distributions of the bellows with different numbers of convolutions. Figure 20 shows the deviations from the bellows to dies. It can be seen from Fig. 19 that the wall thinning region of the multi-convolution bellows is the same as that of the one-convolution bellows, mainly occurring in the crown zone and the straight wall zone between the root and crown. The maximum wall thinning ratios of multi-convolution bellows with convolution numbers from 2, 3 and 4 are 8.77%, 8.8% and 8.95%, respectively, with little difference. Therefore, the number of convolutions has little effect on the maximum wall thinning ratio. It can be seen from Fig. 20 that the variation tendency of the fittability of bellows with multi-convolution is the same as that of the one-convolution. However, the region with the worst fittability occurs in the straight wall zone between the convolutions.

Fig. 24 Point micrometre and Vernier caliper measuring tools
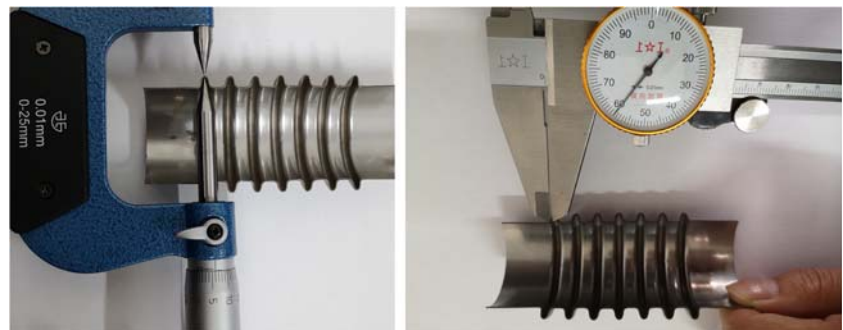
**Table 5** Wall thickness of the simulated and experimental results

Convolution	Measuring point	Simulated result	Experimental result	Error
Left end convolution	A1	0.658 mm	0.622 mm	5.79%
	A2	0.618 mm	0.598 mm	3.30%
	A3	0.596 mm	0.565 mm	5.49%
	A4	0.628 mm	0.595 mm	5.55%
	A5	0.652 mm	0.616 mm	5.80%
Middle convolution	B1	0.695 mm	0.636 mm	9.28%
	B2	0.617 mm	0.584 mm	5.66%
	B3	0.592 mm	0.550 mm	7.64%
	B4	0.618 mm	0.581 mm	6.37%
	B5	0.648 mm	0.616 mm	5.19%
Right end convolution	C1	0.655 mm	0.609 mm	7.55%
	C2	0.631 mm	0.584 mm	8.05%
	C3	0.623 mm	0.572 mm	8.92%
	C4	0.647 mm	0.596 mm	8.56%
	C5	0.662 mm	0.613 mm	8.00%

5.2 Experimental verification

To verify the numerical simulation, the internal pressure adopts a gradient loading path with the forming internal pressure P_f value of 36 MPa in the bulging stage; path 5 is selected for the axial feeding loading path, and the axial feeding is set as 33.6 (7*4.8) mm for seven-convolution bellows hydroforming numerical simulation and experiment. The bellows is obtained, as shown in Fig. 21, and the wall thickness distribution of the

Fig. 25 Comparison of the wall thickness. **a** Left end convolution. **b** Middle convolution. **c** Right end convolution

(a) left end convolution

(b) Middle convolution

(c) Right end convolution
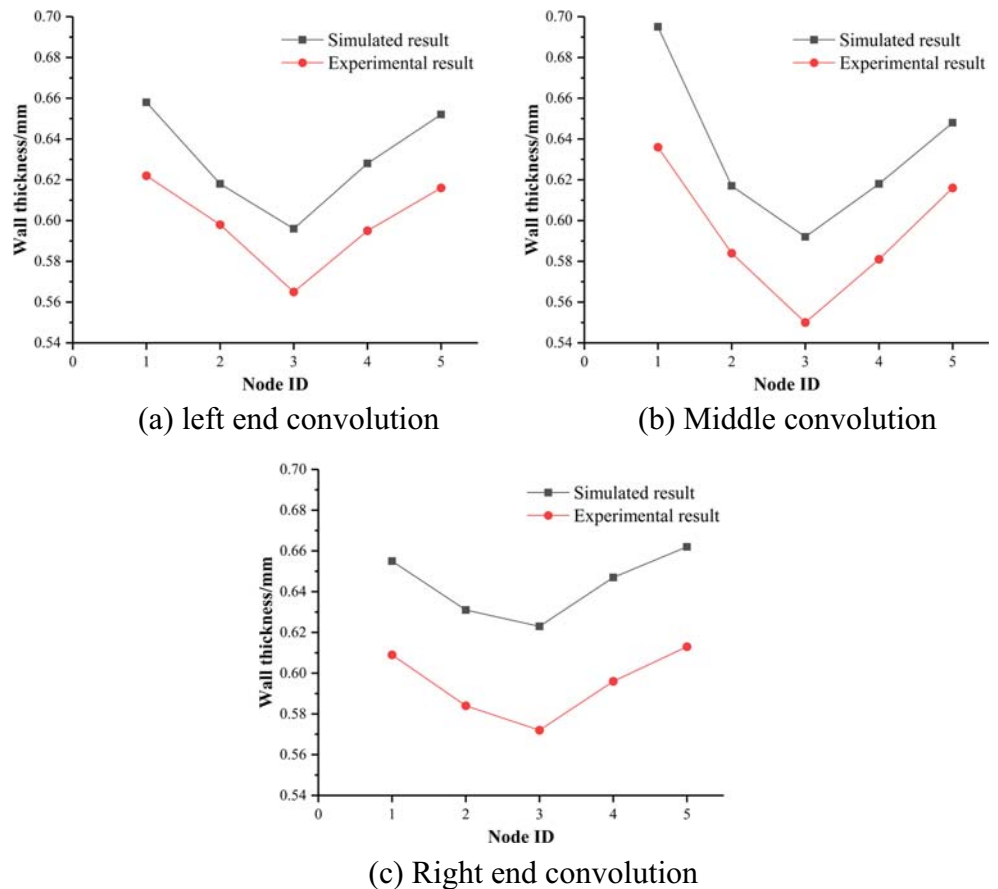
Table 6 Comparison of simulation and test key point coordinate data

| Convolution	Measuring point	Simulated result	Experiment result	Deviation(mm)
Left end convolution	A1	(−2.45, 0)	(−2.5, 0)	0.05
	A2	(−1.3, 1.7)	(−1.4, 1.8)	0.14
	A3	(0, 3. 3)	(0, 3.2)	0.10
	A4	(1.3, 1.7)	(1.4, 1.8)	0.14
	A5	(2.45, 0)	(2.5, 0)	0.05
Middle convolution	B1	(−2.5, 0)	(−2.5, 0)	0
	B2	(−1.35, 1.76)	(−1.5, 1.8)	0.16
	B3	(0, 3.28)	(0, 3.2)	0.08
	B4	(1.35, 1.76)	(1.5, 1.8)	0.16
	B5	(2.5, 0)	(2.5, 0)	0
Right end convolution	C1	(−2.44, 0)	(−2.5, 0)	0.06
	C2	(−1.32, 1.73)	(−1.5, 1.8)	0.19
	C3	(0, 3.26)	(0, 3.2)	0.06
	C4	(1.2, 1.73)	(1.4, 1.8)	0.21
	C5	(2.34, 0)	(2.3, 0)	0.04

simulated bellows is shown in Fig. 22. To measure the thickness distribution of the seven-convolution bellows, it is separated into two halves by a wire electro discharge cutting machine in the diametrical direction. The wall thickness distributions of the leftmost, middle and rightmost convolutions of the bellows are chosen to verify the accuracy of the simulated results. The wall thickness of five key points, including the end point of the root zone, the peak point of the crown zone and the central point of the straight wall zone, is measured, as shown in Fig. 23. Due to the restriction of the convolution structure, the wall thickness of three key points 1, 3 and 5 needs to be measured with a point micrometre. The other two key points 2 and 4 need to be measured with a Vernier caliper, as shown in Fig. 24. The precision of micrometre and Vernier caliper measuring tools used is 0.01 mm, and the accuracy can be estimated to be 0.001 mm. To ensure the accuracy and scientificity of the measurement, the wall thickness

of each key point is measured three times, and the average value is considered as the final result.

The simulated and experimental results are listed in Table 5. To compare the simulation and experimental results more conveniently, the comparison of the wall thickness is shown in Fig. 25. It can be seen from Table 5 and Fig. 25 that the trends of the wall thickness variation results are consistent. The wall thickness of the simulated bellows is generally smaller than the wall thickness of the experimental bellows, and the maximum error is 9.28%. This difference is due to the differences between the experimental and simulation conditions and the possible errors resulting from the measuring instruments and measuring processes. The maximum error is within 10%, which proves that the simulation results are reliable.

To verify the accuracy of the bellows forming precision, a coordinate system, as shown in Fig. 26, is established for each convolution. The deviations of the key points on the convolution, shown in Fig. 23, are measured. The coordinates of key points on the simulated bellows are measured on the neutral layer, and the coordinates of key points on the experimental bellows are measured on the middle layer. The comparison of the coordinates of the key points between the simulated and the experimental bellows is shown in Table 6.

To compare and analyse the results more conveniently, a comparison is displaced in Fig. 27. It can be seen from Table 6 and Fig. 27 that there is a certain deviation in the shape of the bellows formed by simulation and that formed in the experiment. The maximum deviation of the measured key points is 0.21 mm because the tubular blank is modelled with a neutral layer during the hydroforming process, while the neutral layer deviates relative to the intermediate layer after the bellows is formed.
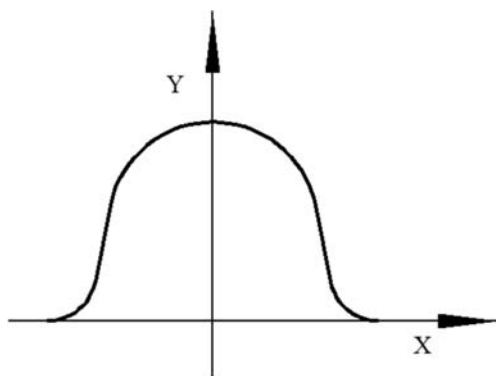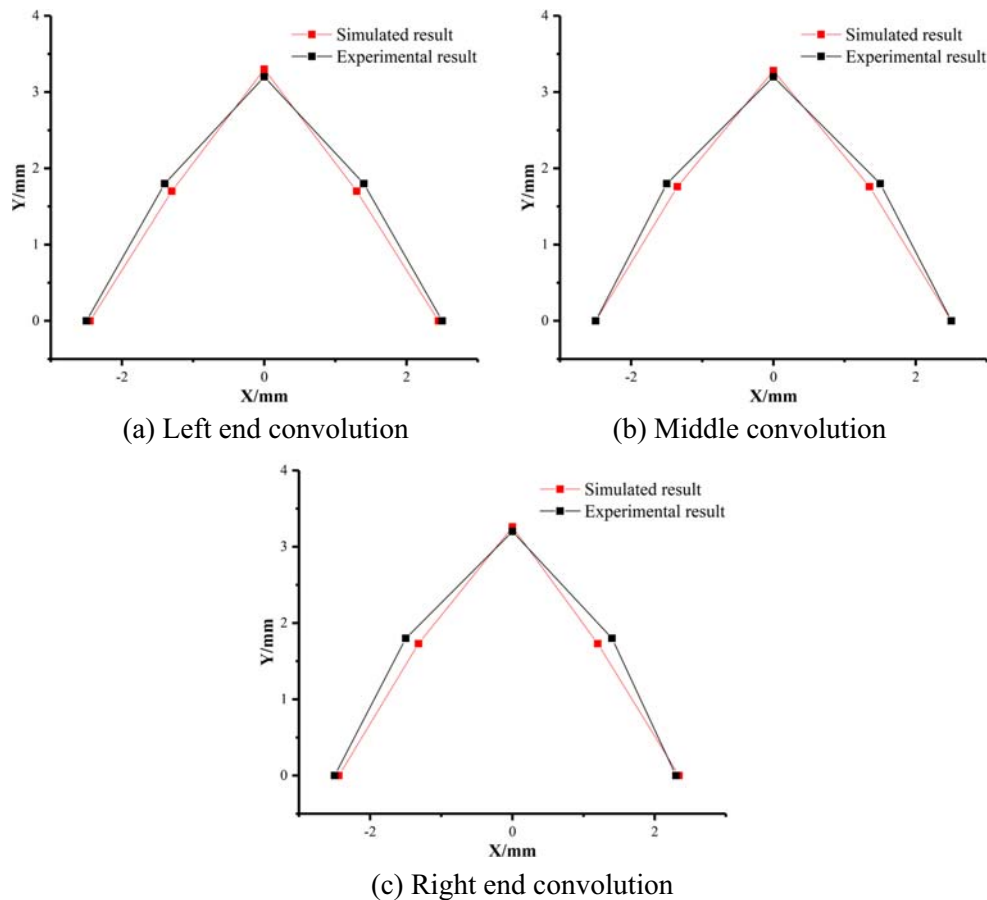

Fig. 26 Coordinate system

Fig. 27 Comparison of the key point coordinate

6 Conclusions

The fittability is presented to evaluate the convolution shape precision of bellows, and the influence of important process parameters on the forming quality of bellows is studied. The conclusions are as follows.

(1) With the increase in internal pressure, the wall thickness of the bellows thins overall, and the fittability of the root zone of the bellows gradually deteriorates. Some region near the crown zone did not fit the dies well when the internal pressure is small.
(2) With the increase in the axial feeding, the wall thinning ratio in some zones decreases, but the wall thickens near the root zone with a tendency of wrinkling. The actual axial feeding should be a bit less than the theoretical axial feeding so as to improve the fittability of the bellows.
(3) When the axial feeding adopts a bilinear loading path, the larger the axial feeding rate in the early period, the smaller the maximum wall thinning ratio. With the increase in axial feeding rate in the early period, the fittability of the bellows roots gradually improves slightly, while the fittability close to the crown zone gradually worsens considerably.

(4) The forming internal pressure needs to increase in multi-convolution bellows hydroforming. The number of convolutions has little effect on the maximum wall thinning ratio. The region with the worst fittability occurs in the straight wall zone between the convolutions.

References

1. Dayyani I, Shaw AD, Flores EIS, Friswell MI (2015) The mechanics of composite corrugated structures: a review with applications in morphing aircraft. Compos Struct 133(1):358–380
2. Kang BH, Lee MY, Shon SM, Moon YH (2007) Forming various shapes of tubular bellows using a single-step hydroforming process. J Mater Process Technol 194(1–3):1–6
3. Bakhshi-Jooybari M, Elyasi M, Gorji A (2010) Numerical and experimental investigation of the effect of the pressure path on forming metallic bellows. J Eng Manuf 224(1):95–101

4. Wei SG, Xu LP, He K, Li JH, Feng W, Du R (2015) Experimental study on manufacturing metal bellows forming by water jet incremental forming. Int J Adv Manuf Technol 81:129–133

5. Wang G, Zhang KF, Wu DZ, Wang JZ, Yu YD (2006) Superplastic forming of bellows expansion joints made of titanium alloys. J Mater Process Techno 178:24–28

6. Zhan M, Shi F, Deng Q, Ma F, Chen JH (2014) Mechanism and law of reducing spinning for coreless die for aluminum alloy corrugated pipe. J Plasticity Eng 21(02):108–115 (in Chinese)

7. Sun L, Lin CY, Fan ZG, Li H, Yao SJ, Wang GD, Chu GC (2019) Experimental and numerical investigation on axial hydro–forging sequence of 6063 aluminum alloy tube. Int J Adv Manuf Technol 105:2869–2877

8. Abrantes JP, Szabo-Ponce A, Batalha GF (2005) Experimental and numerical simulation of tube hydroforming (THF). J Mater Process Technol 164–165:1140–1147

9. Liu J, Li HW, Liu Y, Li LY, Sun C (2018) "Size effect" related hydroforming characteristics of thin-walled 316-L bellow considering pressure change. J Mater Process Technol 98(1–4):505–522

10. Faraji G, Mosavi MM, Norouzifard V (2009) Evaluation of effective parameters in metal bellows forming process. J Mater Process Technol 209(7):3431–3437

11. Yuan Z, Huo SH, Ren JT, Han JF (2019) Study on the hydroforming technology of reinforced s-shaped bellows. Int J Adv Manuf Technol 103(5–8):2541–2552

12. Lee SW (2002) Study on the forming parameters of the metal bellows. J Mater Process Technol 130-131(11):47–53

13. Elyasi M, Bakhshi-Jooybari M, Gorji AH, Nourouzi S, Alinejhad GM (2008) Numerical and experimental investigation on forming metallic bellows in closed and open-die hydroforming. Steel Res Int 79:148–154

14. Prithvirajan R, Sugavaneswaran M, Sathishkumar N, Arumaikkannu G (2019) Metal bellow hydroforming using additive manufactured die: a case study. Rapid Prototyping J 25(4): 765–774

15. Zheng WT, Su M, Zhou LX (2017) Optimization of hydroforming process for titanium alloy TC4 thin-wall corrugated pipe. J Plastics Eng 24(05):52–58 (in Chinese)

16. Faraji G, Besharati MK, Mosavi M, Kashanizadeh H (2008) Experimental and finite element analysis of parameters in manufacturing of metal bellows. Int J Adv Manuf Technol 38: 641–648

17. Zhu Y, Wan M, Zhou YK, Liu QH, Li YC, Zheng NS, Pi KS (2012) Hydroforming of complicated thin-walled circular parts with irregular section by using moving dies. Acta Aeronaut Astronau Sin 33(5):912–919 (in Chinese)

18. Liu J, Wang YL, Li LY, Li X (2017) Influence of process parameters on hydroforming for bi-layered 304 stainless steel bellows. J Plastics Eng 24(4):11–20 (in Chinese)

19. Hao ZL, Xi CY, Huang ZH, Zhang CH, Luo JT (2018) Hydraulic bulging process with axial feedings and strain field of U-shaped metal bellows. J Cent South Univ 25(11):2712–2721

20. Zhang KF, Wang G, Wang GF, Wang CW, Wu DZ (2004) The superplastic forming technology of Ti–6Al–4V titanium alloy bellows. Mater Sci Forum 447–448:247–252

21. Zhang ZC, Furushima T, Manabe K, Tada K, Sasaki O (2015) Development of dieless metal bellows forming process with local heating technique. J Eng Manuf 229(4):664–669

22. Sedighi M, Shamsi M (2017) A new approach in producing metal bellows by local arc heating: a parametric study. Int J Adv Manuf Technol 93:3211–3219

23. Chen J (2015) Numerical simulation and process research of high pressure forming in pipe. Shanghai Jiaotong University, Shanghai (in Chinese)

24. Guo YJ, Wang ZG, Jin GY, Ye SP, Lu ZM, Huang JF, Huang K (2019) Numerical simulation study on the reduction rate of hydroformed bellows. J Zhejiang Univ Technol 47(01):58–62 (in Chinese)